Analysis performance of wavelet OFDM in mobility platforms

Freddy A. Pinto–Benel, Manuel Blanco–Velasco, Fernando Cruz–Roldán *

Department of Teoría de la Señal y Comunicaciones, Escuela Politécnica Superior, Universidad de Alcalá, 28871 Alcalá de Henares, Spain

ARTICLE INFO

ABSTRACT

Wavelet orthogonal frequency division multiplexing (OFDM) is one of the medium access techniques recommended by the IEEE 1901 working group for broadband communications over electrical networks, and is under consideration for IoT applications. This standard provides a flexible architecture supporting integrated access, smart grid, building, in-home, and mobility platform (vehicle) applications. Wavelet OFDM is a filter bank multicarrier system based on the extended lapped transform, in which the transmitting and receiving filters are obtained from a waveform provided by the standard. In this paper, we explore system performance when other waveforms are employed, studying the trade-off between stopband attenuation and transition band width. Furthermore, an alternative and more efficient way of obtaining the theoretical expressions of the achievable data rate is shown, assuming realistic power line communication noise other than additive white Gaussian noise. To demonstrate the capabilities of wavelet OFDM, the results of simulation of the symbol error rate and the data rate in several systems in platform scenarios (in-vehicle and in-aircraft) are shown.

1. Introduction

Communication via electric power lines will play an important and crucial role in the development of intelligent vehicular transport networks [1–6]. For instance, sensors, cameras, connectors, systems for pedestrian and traffic sign detection, and autonomous driving, among other applications, are increasingly important components of the vehicles currently manufactured by the automotive sector and impact their cost, reliability and maintenance. Likewise, in the aeronautic domain there is a trend to replace pneumatic and hydraulic energy sources with electrical ones. However, each electrical system needs a power supply and a communication network [7]. Consequently, the use of power line communications (PLC) may also be extended to mobility platform applications as it combines power and data transmission, thereby simplifying design and reducing development costs and weight.

The IEEE 1901 standard [8] deploys two physical (PHY) layers with two different multicarrier modulations (MCMs): windowed orthogonal frequency division multiplexing (OFDM) and wavelet OFDM [9]. Both technologies have been adopted in the PHY and media access control (MAC) layers of the medium frequency band (less than 15 MHz) broadband power line communication technology for smart grid applications (IEEE 1901.1), and are under consideration for IoT applications (IEEE 1901.3).

Windowed OFDM for PLC has been extensively researched and employed in different fields of communication [10–12]. One important drawback of windowed OFDM is the use of redundant data (usually cyclic prefix), which reduces the achievable data rate. On the contrary, wavelet OFDM has been recommended for the first time in a standard [8], and it deploys two different procedures: baseband and bandpass [9,13]. Wavelet OFDM is a viable and attractive solution for communications over power lines, because it does not require any kind of redundancy and offers higher robustness in noisy environments, greater spectral separation, and reduced adjacent subchannel interference, among other features. Even though the PLC channel is designed for data transmission, wavelet OFDM could be a good alternative for broadband data transmission [9,14,13].

1.1. Motivation and main contributions

Previous studies of wavelet OFDM have focused on the performance of the baseband system in terms of bit error rate (BER) and data rate, assuming different in-home scenarios [9,14]. However, IEEE 1901 is also intended to be applied in platforms (vehicle). In addition, noise sources other than additive white Gaussian noise (AWGN) exist, such as colored background or periodic impulse noise [15–20]. To the best of the authors' knowledge, no prior work has presented an analysis performance of wavelet OFDM focused on in-vehicular communications. As a result, there is currently a lack of research on wavelet OFDM applied in mobility platforms under realistic noise-source conditions.

The main contribution of this paper is threefold. Firstly, several characteristics of the waveforms deployed by IEEE 1901 are analyzed. Specifically, this paper explores the trade-off between the proposed waveforms' stopband attenuation and the transition band width of the frequency response and its influence on system performance in terms of BER and achievable data rate. Secondly, a novel way of obtaining the theoretical expressions that calculate the achievable data rate of wavelet OFDM, assuming channel noise other than AWGN, is presented. Finally, system performance is evaluated considering two different platforms, in-car and in-aircraft, with appropriate noise sources for such scenarios. The study of impulse noise mitigation is out of the scope of this paper. We refer the reader to [20] for more information about this topic.

1.2. Organization and notation

The rest of this paper is organized as follows. A brief discussion of related works is presented in Section 2. In Section 3, the wavelet OFDM transceiver is briefly presented. In Section 4, the theoretical expressions used to calculate the waveforms deployed by the standard and their perfect reconstruction properties are analyzed. Next, the coefficients used to perform 5-tap-per-subcarrier channel equalization are derived in Section 5. The theoretical expressions used to obtain the achievable data rate are detailed in Section 6. Section 7 contains the simulation results considering the waveforms deployed by the standard and other alternative functions. Finally, Section 8 provides our conclusions.

2. Related works

Several researchers have worked in the field of in-vehicle and in-aircraft PLC. Degardin et al. [7] studied a system combining lighting and data communication in the cabin of an aircraft as a first possible application of PLC. Moreover, a software tool simulating PLC communication is presented in [7]. Computer experiments shown that, for the physical layer, bit rates between 18 and 62 Mb/s could be reached. In [2], the results of different measurement campaigns in cabin lighting systems are analyzed. The statistical characteristics of the propagation channels are deduced from the measurements made on a representative test bench. Zheng et al. investigated the time-invariant transmission property through the multibranch naval power network in [1]. In [3], an adaptive impedance-matching system, which improves the communication-signal transfer from the transmitting to the receiving device for vehicular PLC, is presented. The system is evaluated via simulations for a wide range of access-impedance test points and S-parameters of vehicular PLC networks. Authors in [4] proposed a novel method for analytically determining worst case response times of messages for priority-based MAC for the in-car PLC. Furthermore, an algorithm for determining a priority ordering is given in [4]. Pittolo et al. deals with PLC in the context of in-vehicle data networks in [21]. They investigate and assess the similarities and differences among these scenarios, analyzing the channel characteristics in terms of average channel gain, delay spread, coherence bandwidth, and achievable data rate. Recently, the impulsive noise mitigation for OFDM-based in-vehicle PLC systems is studied in [5]. As effective solution, a null subcarriers assisted iterative receiver is proposed. The novel scheme is particularly useful in the presence of narrowband interference.

There have been previous studies of the achievable data rate of OFDM and filter bank multicarrier (FBMC) for PLC. Lin and Siohan derived the capacity of discrete multitone (DMT) in [10]. They obtained theoretical expressions for the interference power of OFDM/OQAM; in addition, the trade-off between spectrum efficiency and the interference power of this FBMC scheme versus DMT, is analyzed. In this work, the communication scenario was different realistic indoor PLC channel environments. Authors in [11] compared the performance of HS/OQAM to windowed OFDM in terms of capacity and throughput in the HomePlug AV context. The achievable data rates for OFDM and different windowed OFDM schemes for arbitrary length channel impulse responses are derived in [22,23]. These studies show a matrix formulation to calculate the intersymbol and the intercarrier interference, and also the noise component at the receiver side. From the above, the signal-to-interference-plus-noise ratio (SINRs) is obtained for different kind of OFDM systems. In [24], this formulation is adapted for narrowband and broadband PLC systems.

The FBMC system deployed in IEEE 1901 is referred to as Wavelet OFDM. However, this denomination is a misnomer, since it is not based on true wavelets implemented in a dyadic filter bank. As it is shown in [9], the baseband scheme is implemented through an extended lapped transform in a transmultiplexer configuration. In [25], the expressions that allow to obtain the coefficients of the prototype filter provided in [8] are derived. The reconstruction properties of the wavelet OFDM transceivers are also studied in the above work. With the aim of keeping spectral efficiency for bandpass communications, the standard [8] deploys a bandpass wavelet OFDM transmitter. This scheme, and also a compatible receiver, is studied in [13]. Several computer simulations are shown, assuming different in-home PLC scenarios. None of these works, however, analyze the performance of wavelet OFDM in mobility platforms.

3. Wavelet OFDM

3.1. Transmitter and receiver systems

Fig. 1 shows the block diagram of the wavelet OFDM transceiver detailed in [9] and considered in this paper. The kth subchannel transmitting filter recommended by the IEEE 1901 standard [8] can be obtained as follows:
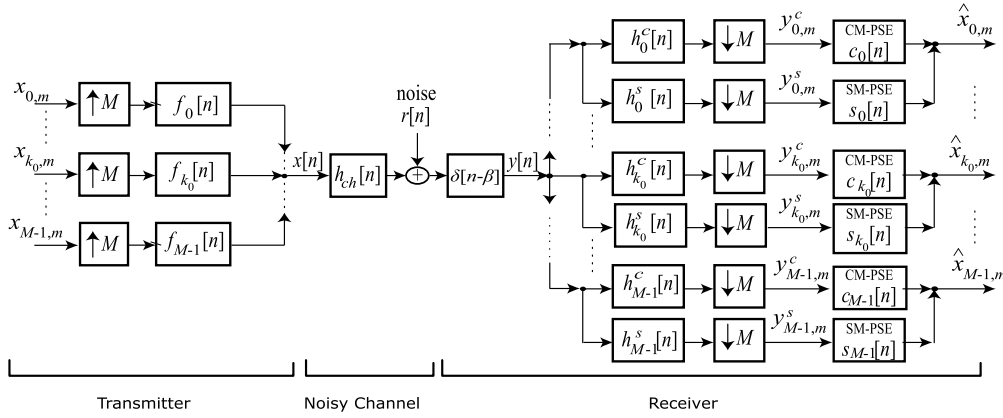
Fig. 1. General block diagram of the wavelet OFDM transceiver with ASCET. CM-PSE and SM-PSE stand for, respectively, cosine-modulated and sine-modulated per subcarrier equalizer.

$$f_k[n] = \sqrt{\frac{2}{M}} \, p[n] \cos\left[\left(k + \frac{1}{2}\right) \frac{\pi}{M} \left(n + \frac{M+1}{2}\right)\right] \cdot \cos(\theta_k), \tag{1}$$

where $0 \le k \le M-1$, $0 \le n \le N$, M is the number of subbands, $p[n]$ is the waveform with order equal to N, and $\theta(k)$ is a phase vector that reduces the peak power. This expression, excluding the term $\cos(\theta_k)$, corresponds to the synthesis filters of an extended lapped transform (ELT) introduced by H. Malvar [26].

The receiver system can be implemented as the time reflection of the transmitting filters [9]:

$$h_k^c[n] = \sqrt{\frac{2}{M}} \, p[n] \cos\left[\left(k + \frac{1}{2}\right) \frac{\pi}{M} \cdot \left(N - 1 - n + \frac{M+1}{2}\right)\right] \cdot \cos(\theta_k), \tag{2}$$

and, in addition, a set of sine-modulated filter bank (SMFB) receiving filters whose impulse response are given by

$$h_k^s[n] = \sqrt{\frac{2}{M}} \, p[n] \sin\left[\left(k + \frac{1}{2}\right) \frac{\pi}{M} \cdot \left(N - 1 - n + \frac{M+1}{2}\right)\right] \cdot \cos(\theta_k). \tag{3}$$

Both filter banks (see Fig. 1) form the so-called adaptive sine-modulated/cosine-modulated filter bank equalizer for transmultiplexer (AS-CET) system. In this work, the ASCET is employed to compensate for the channel effects, such as in [9,25,14].

4. Analysis of the waveforms

The IEEE 1901 standard deploys wavelet OFDM transceivers with different numbers of subchannels: $M = 512$, 1024, and 2048. It is important to notice that the proposed filter bank multicarrier system is not based on a dyadic system with true wavelet, but on an ELT with a transmulplexer configuration [9]. For the above, waveforms with lengths $L = 2\,mM$ (where $m = 2, 3, 4$ is the overlapping factor) are also included in [8]. In this paper, we focus on the characteristics of the waveforms where $m = 2$.

The standard defines an initial mother filter $h[n]$ from which the waveform or prototype filter $p[n]$ can be obtained [8, pp. 1205]. However, the standard does not provide expressions that allow designers to obtain the corresponding coefficients quickly. We have derived from [25] that the waveforms belong to a parametrized family of windows proposed by H. Malvar [26], the coefficients of which can be generated as follows:

$$p[n] = \cos(\theta_{n0}) \cdot \cos(\theta_{n1}), \tag{4a}$$

$$p[M - 1 - n] = \sin(\theta_{n0}) \cdot \cos(\theta_{n1}), \tag{4b}$$

$$p[M + n] = \cos(\theta_{n0}) \cdot \sin(\theta_{n1}), \tag{4c}$$

$$p[2M - 1 - n] = -\sin(\theta_{n0}) \cdot \sin(\theta_{n1}), \tag{4d}$$

for $n = 0, 1, \ldots, \frac{M}{2} - 1$, where

$$\theta_{n0} = -\frac{\pi}{2} + \kappa_{n + \frac{M}{2}}, \tag{5a}$$

$$\theta_{n1} = -\frac{\pi}{2} + \kappa_{\frac{M}{2} - 1 - n}, \tag{5b}$$

and

$$\kappa_q = \left[\left(\frac{1 - \gamma}{2M}\right)(2q + 1) + \gamma\right] \frac{(2q + 1)\pi}{8M}. \tag{6}$$

We have observed that the waveforms deployed by [8] are identical to Malvar's prototype filters with the parameter $\gamma = 0.3$, for $M = 512$, 1024, and 2048. This parameter γ typically varies in the range $[0, 1]$ and controls the trade-off between the stopband attenuation
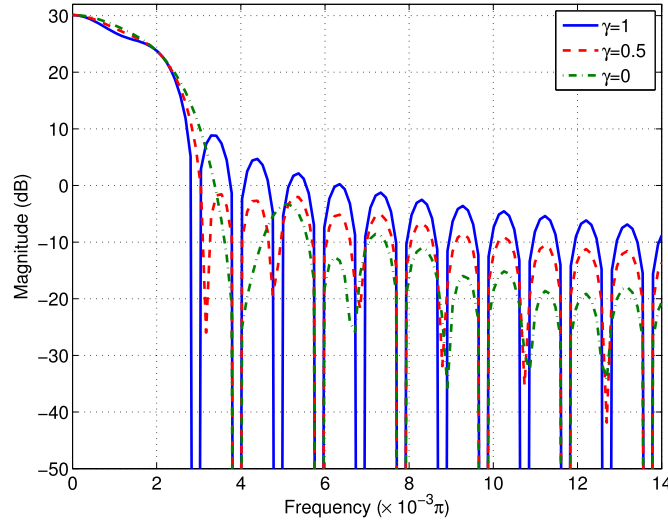
Fig. 2. Comparison between the first subband filter for $M = 512$, $\gamma = 1$, $\gamma = 0.5$ and $\gamma = 0$.

and the transition band width of the waveform frequency responses. The higher the γ value, the greater the stopband energy and the lower the transition band width. Fig. 2 shows a comparison of the aforementioned properties.

We also studied in [25] whether the wavelet OFDM transceiver satisfies the perfect reconstruction (PR) property. This property implies that each $\hat{x}_{k_0,m}$ output is, in the absence of channel, equalizer, and noise, a delayed version of the input signal $x_{k_0,m}$ multiplied by a constant. The conditions necessary to fulfill the PR property are presented in [26] and require the waveform to be even-symmetric and to satisfy the following condition set:

$$\sum_{i=0}^{2m-2s-1} p[n + iM]p[n + i + 2sM] = \delta[s], \tag{7}$$

where $n = 0, 1, \ldots, \frac{M}{2} - 1$ and $s = 0, \cdots, m - 1$. In the equation above, when $m = 2$ is replaced, we obtain

$$p^2[n] + p^2[n + M] + p^2[n + 2M] + p^2[n + 3M] = 1, \tag{8a}$$

$$p[n]p[n + 2M] + p[n + M]p[n + 3M] = 0. \tag{8b}$$

In the case of the IEEE 1901 standard [8], the waveform presents even symmetry, i.e., the prototype filter is linear-phase. In addition, using the transmitting and receiving filters given by (1)-(2), respectively, we performed computer simulations to test whether the other two conditions (8a)-(8b) are also fulfilled. These can be found in more detail in [25].

5. Channel equalization with 2-ASCET

Fig. 1 also depicts the receiver system that performs channel equalization through finite impulse response (FIR) filters $c_k[n]$ and $s_k[n]$. The non-causal versions of these filters are defined as

$$c_k[n] = \sum_{\mu=-L_A}^{L_A} c_{\mu,k} \cdot \delta[n - \mu], \tag{9}$$

$$s_k[n] = \sum_{\mu=-L_A}^{L_A} s_{\mu,k} \cdot \delta[n - \mu], \tag{10}$$

where $2 \cdot L_A + 1$ is the number of taps of each FIR filter. In [9], the expressions to obtain the coefficients corresponding to the zero-order (0-ASCET) and one-order (1-ASCET) FIR filters are derived. The coefficients of the corresponding 5-tap FIR filters (2-ASCET) are initially obtained in [27]. For this case, let us consider the following system function:

$$E_k(z) = \psi_{0,k}z^2 + \psi_{1,k}z + \psi_{2,k} + \psi_{3,k}z^{-1} + \psi_{4,k}z^{-2}. \tag{11}$$

By performing a similar analysis to [9,27], the following can be derived:

$$\psi_{0,k} = \frac{1}{4}\left[(\eta_{1k} - 2\eta_{2k} + \eta_{3k}) + \frac{\sqrt{2}}{2}(-\eta_{0k} + 2\eta_{1k} - 2\eta_{2k} + 2\eta_{3k} - \eta_{4k}) + j\left(-\eta_{1k} + \eta_{3k} + \frac{\sqrt{2}}{2}(\eta_{ok} - \eta_{4k})\right)\right], \tag{12a}$$

$$\psi_{1,k} = \pm\frac{1}{4}\left[\eta_{0k} - \eta_{4k} - j(\eta_{0k} - 2\eta_{1k} + 2\eta_{2k} - 2\eta_{3k} + \eta_{4k}) \cdot \left(1 + \sqrt{2}\right)\right], \tag{12b}$$

$$\psi_{2,k} = \frac{1}{2}\left[(\eta_{0k} - \eta_{1k} + 2\eta_{2k} - \eta_{3k} + \eta_{4k}) + \frac{\sqrt{2}}{2}(\eta_{0k} - 2\eta_{1k} + 2\eta_{2k} - 2\eta_{3k} + \eta_{4k})\right], \tag{12c}$$

$$\psi_{3,k} = \pm\frac{1}{4}\left[\eta_{0k} - \eta_{4k} + j(\eta_{0k} - 2\eta_{1k} + 2\eta_{2k} - 2\eta_{3k} + \eta_{4k})\cdot\left(1 + \sqrt{2}\right)\right], \tag{12d}$$

$$\psi_{4,k} = \frac{1}{4}\left[(\eta_{1k} - 2\eta_{2k} + \eta_{3k}) + \frac{\sqrt{2}}{2}(-\eta_{0k} + 2\eta_{1k} - 2\eta_{2k} + 2\eta_{3k} - \eta_{4k}) - j\left(-\eta_{1k} + \eta_{3k} + \frac{\sqrt{2}}{2}(\eta_{ok} - \eta_{4k})\right)\right], \tag{12e}$$

where

$$\eta_{ik} = \frac{H_{ch}^*\left(e^{j\frac{\pi}{8M}(4k+i)}\right)}{\left|H_{ch}\left(e^{j\frac{\pi}{8M}(4k+i)}\right)\right|^2 + \frac{1}{SNR}},$$

for $i = 0, 1, 2, 3, 4$. Furthermore, $H_{ch}(e^{j\Omega})$ is the channel frequency response and SNR is the signal-to-noise ratio. Once the above coefficients are obtained, we obtain

$$c_{\mu,k} = \Re\{\psi_{\mu+2,k}\}, \tag{13a}$$

$$s_{\mu,k} = \Im\{\psi_{\mu+2,k}\}, \tag{13b}$$

where $\Re\{\cdot\}$ and $\Im\{\cdot\}$ represent the real and the imaginary part, respectively.

6. Data rate

Broadband power line applications demand both low BER and high-speed data transmission. In this sense, the data rate under realistic conditions provides an important measurement for comparing the performance of different systems. The expressions used to determine the theoretical data rate of wavelet OFDM, assuming AWGN, are derived in [14]. In this section, we show an alternative derivation based on the transfer function that relates any subcarrier input on the transmitter side to any subcarrier output at the receiver. In addition, the PLC noise under consideration is different to AWGN. We remark that the obtained expressions are not only valid for wavelet OFDM, but also are applicable to maximally decimated filter bank multicarrier systems with a scheme similar to Fig. 1.

The discrete-time transmitted signal can be expressed in the z-domain as follows:

$$X(z) = \sum_{k=0}^{M-1} F_k(z)\cdot X_k\left(z^M\right), \tag{14}$$

where $F_k(z)$ is the system function of each filter given in (1).

Let us consider channel impulse response and channel noise in the z-domain, respectively expressed as $H_{ch}(z)$ and $R(z)$. The first block on the receiver side introduces a delay of β samples, so the received signal can be written as

$$Y(z) = X(z)\cdot H_{ch}(z)\cdot z^{-\beta} + R(z)\cdot z^{-\beta}. \tag{15}$$

The i-th output of the synthesis CMFB in the absence of noise can be expressed in the z-domain as

$$\begin{aligned}
Y_i^c(z) &= \frac{1}{M}\sum_{l=0}^{M-1} H_i^c\left(z^{\frac{1}{M}}W^l\right)Y\left(z^{\frac{1}{M}}W^l\right) \\
&= \frac{1}{M}\sum_{l=0}^{M-1} H_i^c\left(z^{\frac{1}{M}}W^l\right)X\left(z^{\frac{1}{M}}W^l\right)\cdot H_{ch}\left(z^{\frac{1}{M}}W^l\right)\left(z^{\frac{1}{M}}W^l\right)^{-\beta} \\
&= \frac{1}{M}\sum_{l=0}^{M-1} H_i^c\left(z^{\frac{1}{M}}W^l\right)\left[\sum_{k=0}^{M-1} F_k\left(z^{\frac{1}{M}}W^l\right)\cdot X_k\left(\left(z^{\frac{1}{M}}W^l\right)^M\right)\right]\cdot H_{ch}\left(z^{\frac{1}{M}}W^l\right)z^{-\frac{\beta}{M}}W^{-l\beta},
\end{aligned} \tag{16}$$

where $W = e^{-j\frac{2\pi}{M}}$ and $H_i^c(z)$ is the z-transform of the filters given by (2). Rearranging the terms obtains

$$\begin{aligned}
Y_i^c(z) &= \frac{1}{M}\sum_{l=0}^{M-1} H_i^c\left(z^{\frac{1}{M}}W^l\right)\cdot\left[\sum_{k=0}^{M-1} F_k\left(z^{\frac{1}{M}}W^l\right)\cdot X_k(z)\right]\cdot H_{ch}\left(z^{\frac{1}{M}}W^l\right)z^{-\frac{\beta}{M}}W^{-l\beta} \\
&= \frac{1}{M}\sum_{k=0}^{M-1} X_k(z)\sum_{l=0}^{M-1} H_i^c\left(z^{\frac{1}{M}}W^l\right)\cdot F_k\left(z^{\frac{1}{M}}W^l\right)H_{ch}\left(z^{\frac{1}{M}}W^l\right)z^{-\frac{\beta}{M}}W^{-l\beta}.
\end{aligned} \tag{17}$$

Then, defining the transfer function $T_{i,k}^c(z) = H_i^c(z)F_k(z)H_{ch}(z)$ obtains

$$Y_i^c(z) = \frac{1}{M}\sum_{k=0}^{M-1} X_k(z)\sum_{l=0}^{M-1} T_{i,k}^c\left(z^{-\frac{1}{M}}W^l\right)z^{-\frac{\beta}{M}}W^{-l\beta} = \sum_{k=0}^{M-1} X_k(z)U_{i,k}^c(z). \tag{18}$$

Notice that the relation in the time-domain between $U_{i,k}^c(z)$ and $T_{i,k}^c(z)$ is given by $u_{i,k}^c[n] = t_{i,k}^c[nM - \beta]$, i.e., $u_{i,k}^c[n]$ is a delayed and decimated version of $t_{i,k}^c[n]$.

Following the same reasoning, the ith output of the synthesis SMFB is given by

$$Y_i^s(z) = \frac{1}{M} \sum_{k=0}^{M-1} X_k(z) \sum_{l=0}^{M-1} T_{i,k}^s\left(z^{-\frac{1}{M}} W^l\right) z^{-\frac{\beta}{M}} W^{-l\beta} = \sum_{k=0}^{M-1} X_k(z) U_{i,k}^s(z), \tag{19}$$

where $T_{i,k}^s(z) = H_i^s(z) F_k(z) H_{ch}(z)$, $H_i^s(z)$ is the z-transform of the filters given by (3), and $u_{i,k}^s[n] = t_{i,k}^s[nM - \beta]$.

It is important to highlight that when the subchannel filters show high selectivity and discrimination between subcarriers, the functions $t_{i,k}^c[nM - \beta]$ and $t_{i,k}^s[nM - \beta]$ are nearly zero when $k \neq i - 1, i$, and $i + 1$.

Next, assuming that an L_A-ASCET is chosen as the channel equalization technique, the ith demodulated symbol can be written as

$$\hat{X}_i(z) = Y_i^c(z) C_i(z) + Y_i^s(z) S_i(z) = \sum_{k=0}^{M-1} X_k(z) \left(U_{i,k}^c(z) C_i(z) + U_{i,k}^s(z) S_i(z) \right) = \sum_{k=0}^{M-1} X_k(z) V_{i,k}(z), \tag{20}$$

where $C_i(z)$ and $S_i(z)$ are, respectively, the z-transform of $c_i[n]$ and $s_i[n]$, previously defined in (9)-(10). Then, the reconstructed symbol can be rewritten as

$$\hat{X}_i(z) = X_i(z) V_{i,i}(z) + \sum_{\substack{k=0 \\ k \neq i}}^{M-1} X_k(z) V_{i,k}(z), \tag{21}$$

and expressed in time-domain terms as

$$\hat{x}_i[n] = \sum_{\ell} v_{i,i}[\ell] \cdot x_i[n - \ell] + \sum_{\substack{k=0 \\ k \neq i}}^{M-1} \sum_{\ell} v_{i,k}[\ell] \cdot x_i[n - \ell]$$

$$= v_{i,i}[0] \cdot x_i[n] + \underbrace{\sum_{\substack{\ell \\ \ell \neq 0}} v_{i,i}[\ell] \cdot x_i[n - \ell]}_{\text{ISI}} + \underbrace{\sum_{\substack{k=0 \\ k \neq i}}^{M-1} \sum_{\ell} v_{i,k}[\ell] \cdot x_i[n - \ell]}_{\text{ICI}}, \tag{22}$$

where ISI and ICI denote, respectively, the intersymbol and the intercarrier interference.

The power of the ith subcarrier signal can be calculated as

$$P_\gamma(i) = \sigma_x^2 \left| v_{i,i}[0] \right|^2. \tag{23}$$

Similarly, the power corresponding to the intersymbol and intercarrier interference of the ith subcarrier ($P_{ISI}(i)$ and $P_{ICI}(i)$) can be obtained as

$$P_{INT}(i) = P_{ISI}(i) + P_{ICI}(i) = \sigma_x^2 \left(\sum_{\substack{\ell \\ \ell \neq 0}} \left| v_{i,i}[\ell] \right|^2 + \sum_{\substack{k=0 \\ k \neq i}}^{M-1} \sum_{\ell} \left| v_{i,k}[\ell] \cdot \right|^2 \right). \tag{24}$$

The noise at the ith output of the synthesis CMFB/SMFB can be calculated as

$$\Upsilon_i^c(z) = \frac{1}{M} \sum_{l=0}^{M-1} H_i^c\left(z^{\frac{1}{M}} W^l\right) R\left(z^{\frac{1}{M}} W^l\right) z^{-\frac{\beta}{M}} W^{-l\beta}$$

$$= \frac{1}{M} \sum_{l=0}^{M-1} \Gamma_{i,k}^c\left(z^{-\frac{1}{M}} W^l\right) z^{-\frac{\beta}{M}} W^{-l\beta}, \tag{25}$$

and

$$\Upsilon_i^s(z) = \frac{1}{M} \sum_{l=0}^{M-1} H_i^s\left(z^{\frac{1}{M}} W^l\right) R\left(z^{\frac{1}{M}} W^l\right) z^{-\frac{\beta}{M}} W^{-l\beta}$$

$$= \frac{1}{M} \sum_{l=0}^{M-1} \Gamma_{i,k}^s\left(z^{-\frac{1}{M}} W^l\right) z^{-\frac{\beta}{M}} W^{-l\beta}, \tag{26}$$

respectively, where $\Gamma_i^c(z) = H_i^c(z)R(z)$ and $\Gamma_i^s(z) = H_i^s(z)R(z)$. In the time-domain, (25) and (26) can be expressed as

$$r_i^c[n] = \sum_t h_i^c[t] \cdot r[nM - t - \beta],$$
(27)

$$r_i^s[n] = \sum_t h_i^s[t] \cdot r[nM - t - \beta].$$
(28)

Therefore, the noise at the ith demodulated symbol is

$$\sum_{\mu=-L_A}^{L_A} r_i^c[n-\mu] \cdot c_{i,\mu} + r_i^s[n-\mu] \cdot s_{i,\mu}.$$
(29)

The power noise calculation is detailed in Appendix A. Assuming that the PLC noise is a stationary stochastic process, the equation for the power noise (A.5) can be expressed as

$$P_r(i) = \sum_{\mu_1=-L_A}^{L_A} \sum_{\mu_2=-L_A}^{L_A} \left[\sum_{t_1} \sum_{t_2} R_r(\tau) \left(c_{i,\mu_1} c_{i,\mu_2} \cdot h_i^c[t_1] h_i^c[t_2] + s_{i,\mu_1} s_{i,\mu_2} h_i^s[t_1] h_i^s[t_2] + 2c_{i,\mu_1} s_{i,\mu_2} h_i^c[t_1] h_i^s[t_2] \right) \right],$$
(30)

where $\tau = (t_2 - t_1) + M(\mu_2 - \mu_1)$. Observe that if the PLC noise is AWGN, (A.5) can be simplified to [14, eq. (54)]:

$$P_r(k_0) = \sigma_r^2 \sum_{t=0}^{N+2L_A} \left| h_{k_0,\mu}^c[t] + h_{k_0,\mu}^s[t] \right|^2,$$
(31)

where

$$h_{k_0,\mu}^c[n] = h_{k_0}^c[n] * c_k[n],$$

$$h_{k_0,\mu}^s[n] = h_{k_0}^s[n] * s_k[n].$$

With the above powers, the signal-to-interference plus noise ratio (SINR) can be calculated as

$$\text{SINR}(i) = \frac{P_\gamma(i)\sigma_x^2}{P_{ICI+ISI}(i) + P_r(i)}.$$
(32)

Finally, the achievable data rate with wavelet OFDM can be obtained as

$$T_R = \sum_{m=0}^{M-1} \Delta_f \cdot C(i),$$
(33)

where Δ_f is the frequency spacing and $C(i)$ is the data rate for the ith subcarrier:

$$C(i) = \log_2 \left(1 + \frac{\text{SINR}(i)}{\chi} \right).$$
(34)

χ is the SINR gap, which for PAM modulation is given by

$$\chi = \frac{1}{3} \left[Q^{-1} \left(\frac{SER}{2} \right)^2 \right],$$
(35)

where SER is the symbol error rate and Q^{-1} is the inverse tail probability of the standard normal distribution.

7. Simulation results

In this section, we study the performance of wavelet OFDM through computer simulation. Specifically, we have designed five different waveforms using (4)-(6) for the following γ values[1]: 0, 0.3, 0.5, 0.75 and 1. The wavelet OFDM transceiver presents $M = 512$ subcarriers for all the simulations, with only 360 active subcarriers, as recommended in the standard in the 2 MHz to 28 MHz frequency range. The frequency spacing $\triangle f = 61.035$ KHz is also defined in [8]. Equalization is carried out using FIR filters $c_k[n]$ and $s_k[n]$ with 1 (0-ASCET) and 5 (2-ASCET) coefficients. Using the above parameters, we calculated the achievable data rate. In addition, we obtained the bit error rate through Monte Carlo simulations. In this case, the transceiver includes a concatenated encoder with a forward error correction (FEC) block and a codification rate of 1/2. In our experiments, the channel remains constant during each multicarrier symbol, perfect synchronization and channel knowledge are assumed at the receiver and 2-PAM is used as primary mapping. Finally, the average signal-to-noise ratio (SNR) is obtained from the receiver side as follows [11]:

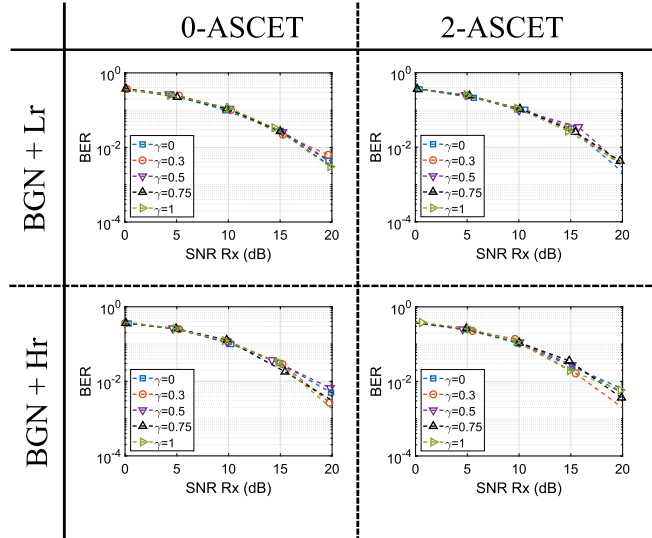[1] The standard [8] deploys a waveform with $\gamma = 0.3$.

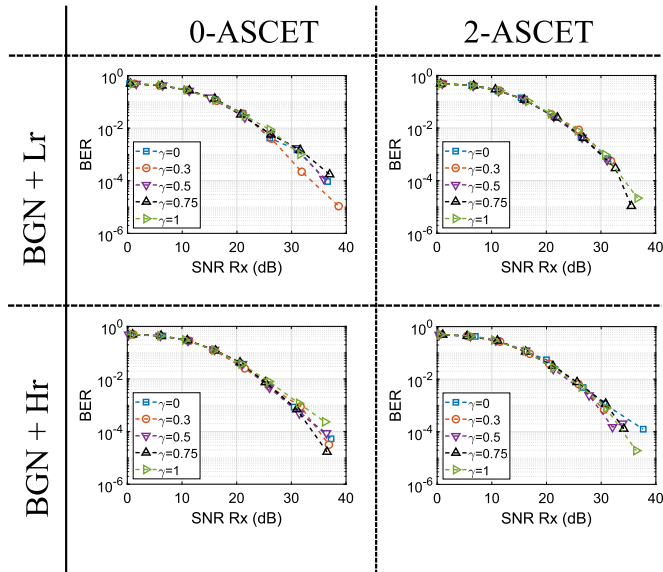**Fig. 3.** BER for different in-car PLC channels, noise and equalizers (2-PAM constellation).

Fig. 4. BER for different in-car PLC channels, noise and equalizers (8-PAM constellation).

$$\mathrm{SNR_{RX}} = 10\log_{10}\left(\frac{1}{M_{ac}}\sum_{k\in\mathbb{K}_{on}}\frac{|H_{ch}(k)|^2\sigma_x^2(k)}{\sigma_n^2(k)}\right), \tag{36}$$

where $H_{ch}(k)$ is the frequency channel coefficient and $\sigma_x^2(k)$ and $\sigma_n^2(k)$ denote, respectively, the signal and the noise powers at the k-th subcarrier. In our simulations, we accounted for the spectral mask specified in the IEEE 1901 standard [8, Table 14-14], which limits the PSD of the transmitted signal to -55 dBm/Hz.

7.1. In-vehicle scenario

In these experiments, 100 realizations of an in-car PLC channel model that considers different sections and states of a 2006 Pontiac Solstice are used. We refer the reader to [28] for more information about the channel measurements. As PLC noise, the study considers various sources. First, it includes background noise (BGN), modeled as in [28] by Gaussian noise with a PSD between -140 dBm/Hz and -120 dBm/Hz. In our case, a PSD equal to -120 dBm/Hz has been assumed, since it is the worst case scenario. Second, periodic impulsive noise with both a high repetition rate (Hr) and a low repetition rate (Lr), as in [29], is also used to model in-car PLC impulsive noise.

Fig. 3 depicts the BER obtained under the conditions above and assuming 2-PAM. Only for high SNR values can small deviations be observed for the different waveforms, the one recommended in the standard ($\gamma = 0.3$) being the one that performs best in terms of BER. This same conclusion holds under 8-PAM (see Fig. 4). Irrespective, the difference between best and worst performance is not significant. However, the results obtained for the achievable data rate with 2-ASCET reveal differences depending on the γ parameter used for the waveform. Fig. 5 shows the resulting data rate, considering a constellation of infinite granularity, for different values of γ. The findings of these simulations show that $\gamma = 1$ achieves the highest value in almost every case. In fact, the data rates obtained from $\gamma = 1$ with
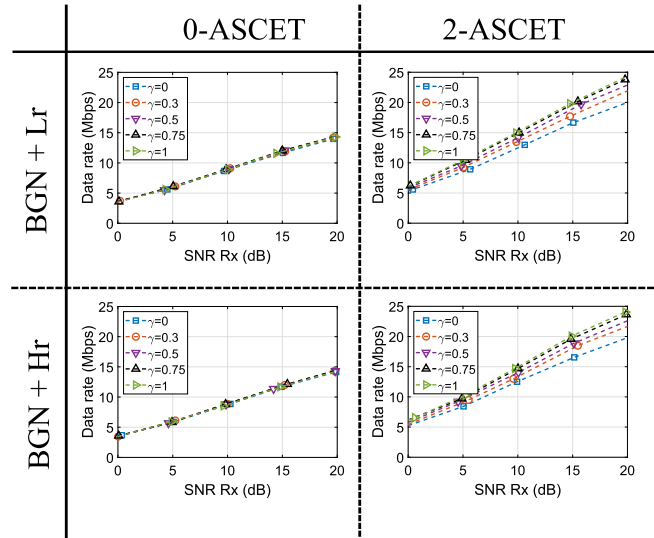
Fig. 5. Achievable data rate for different in-car PLC channels, noise and equalizers.
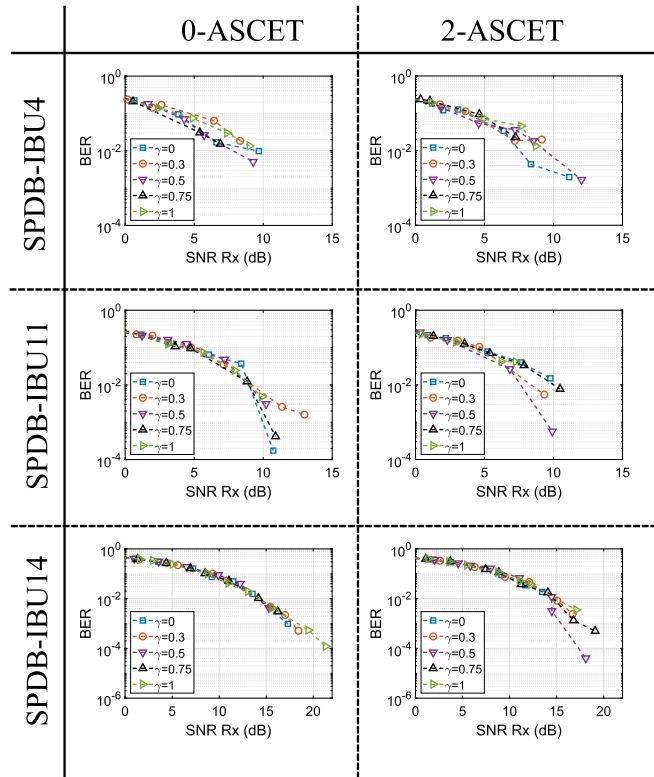

Fig. 6. BER for different in-aircraft PLC channels, noise and equalizers (2-PAM constellation).

different noise sources and assuming a 2-ASCET equalizer (left column) are 11.95%, 11.62% and 9.41% higher than those obtained with the waveform deployed by the standard.

7.2. In-aircraft scenario

In this set of simulations, we employ an in-aircraft PLC channel model which represents the connection between the Secondary Power Distribution Box (SPDB) and various illumination ballast units (IBU) [7,2]. Specifically, two short lines (SPDB-IBU1 and SPDB-IBU4) and two long lines (SPBDB-IBU11 and SPDB-IBU14) are used. A detailed discussion of these PLC channels can be found in [7,2]. Regarding the PLC noise, the experiments also include BGN, modeled as in [28] by Gaussian noise with a PSD of −120 dBm/Hz. Likewise, periodic impulsive noise with both a high repetition rate (PINH) and a low repetition rate (PINL) is also added at the receiver. For the in-aicraft scenario, [2] suggests that, in a differential-mode configuration, the noise can be modeled by means of a white band noise generator with a current
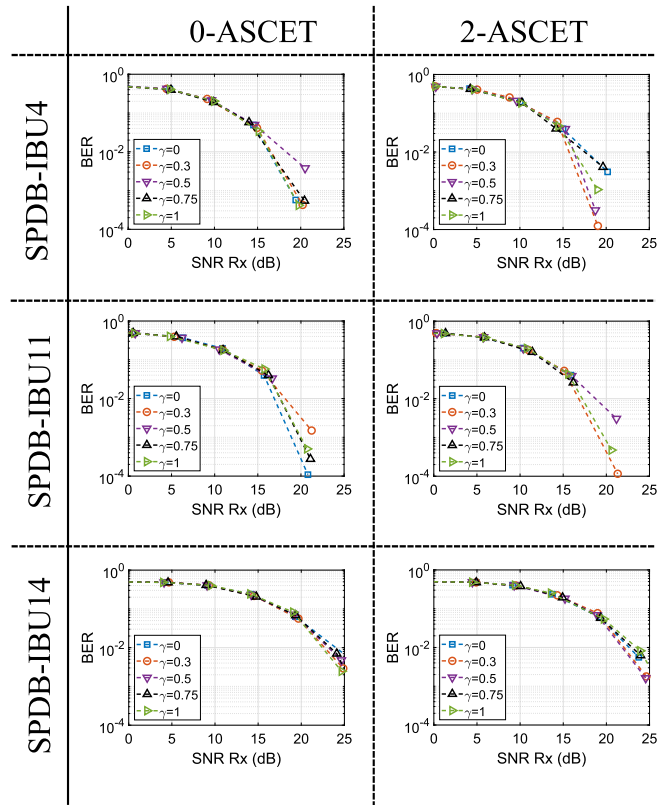
Fig. 7. BER for different in-aircraft PLC channels, noise and equalizers (8-PAM constellation).
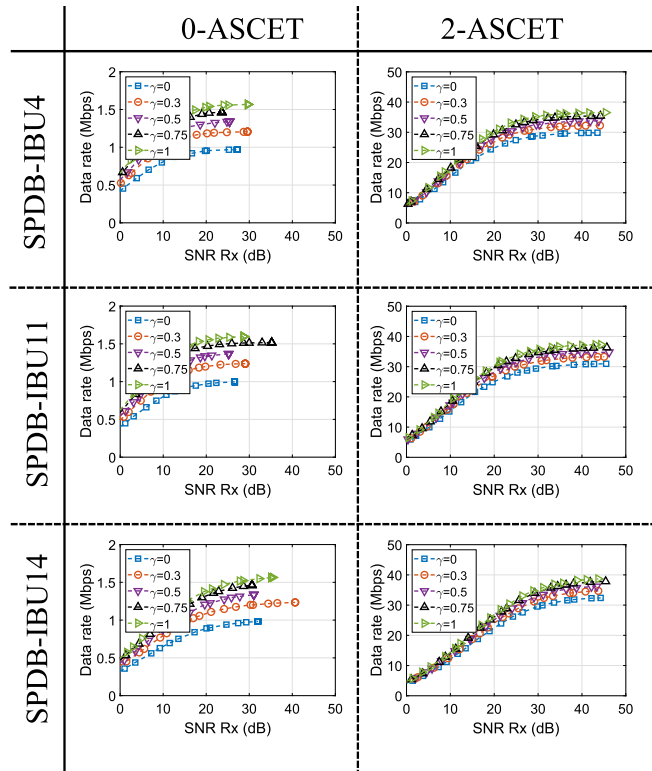

Fig. 8. Achievable data rate for various in-aircraft PLC channels, noise and equalizers.

noise density equal to -8 dBμA/KHz (equivalent to a PSD equal to -111 dBm/Hz on 50Ω) and the signal power can reach 45 dBμA/KHz (equivalent to -58 dBm/Hz). Therefore, AWGN with a PSD set at -111 dBm/Hz has been chosen.

Figs. 6 and 7 show the results obtained under the above-mentioned conditions, assuming 2-PAM and 8-PAM, respectively. As in the previous simulation, no single solution provides the best result, since in every case a waveform with a different γ value achieves the best performance. Once again, the difference between the worst and the best result is not significant.

Fig. 8 depicts the resulting system data rate. As can be seen, the waveform with $\gamma = 1$ outperforms the other cases. In fact, considering the SPBD-IBU14 PLC channel and the 0- and 2-ASCET, the waveform with $\gamma = 1$ increases the data rate by 27.76% and 11.47%, respectively. From the achieved results, it can be seen that both the complexity of the equalizer and the γ value have again a significant impact on the achievable data rate.

8. Conclusion

This paper presents a novel study of the performance of broadband PLC using wavelet OFDM in mobility platforms. First, the characteristics of several waveforms of potential use in design of the wavelet OFDM are presented. Second, the coefficients of the 2-ASCET equalizer are shown and the theoretical expressions with which to obtain the achievable data rate for all types of noise are derived. Next, several simulations are carried out to verify the performance in terms of BER and data rate. Two kinds of mobility platforms are considered: in-car and in-aircraft. In these scenarios, the influence of the γ parameter, which allows modification of the stopband attenuation and the transition band width of the waveform, is tested. Two conclusions may be drawn from these outcomes: first, wavelet OFDM is a good alternative for communications on different platforms; and second, waveforms other than that deployed by the standard can provide the best data rate results.

Declaration of competing interest

The authors declare that they have no known competing financial interests or personal relationships that could have appeared to influence the work reported in this paper.

Acknowledgement

Appendix A. Noise power derivation

Since the noise power is equal to the second central moment of (29), it yields

$$
\begin{aligned}
P_r(i) =& E\left[\left|\sum_{\mu=-L_A}^{L_A} r_i^c[n-\mu]c_{i,\mu} + r_i^s[n-\mu]s_{i,\mu}\right|^2\right] \\
=& E\left[\left(\sum_{\mu_1=-L_A}^{L_A} r_i^c[n-\mu_1]\cdot c_{i,\mu_1} + r_i^s[n-\mu_1]\cdot s_{i,\mu_1}\right)\left(\sum_{\mu_2=-L_A}^{L_A} r_i^c[n-\mu_2]\cdot c_{i,\mu_2} + r_i^s[n-\mu_2]\cdot s_{i,\mu_2}\right)^*\right] \\
=& \sum_{\mu_1=-L_A}^{L_A}\sum_{\mu_2=-L_A}^{L_A} c_{i,\mu_1}c_{i,\mu_2}\cdot E\left[r_i^c[n-\mu_1]\left(r_i^c[n-\mu_2]\right)^*\right] + 2\sum_{\mu_1=-L_A}^{L_A}\sum_{\mu_2=-L_A}^{L_A} c_{i,\mu_1}s_{i,\mu_2}\cdot E\left[r_i^c[n-\mu_1]\left(r_i^s[n-\mu_2]\right)^*\right] \\
& + \sum_{\mu_1=-L_A}^{L_A}\sum_{\mu_2=-L_A}^{L_A} s_{i,\mu_1}s_{i,\mu_2}\cdot E\left[r_i^s[n-\mu_1]\left(r_i^s[n-\mu_2]\right)^*\right],
\end{aligned}
\tag{A.1}
$$

where

$$
\begin{aligned}
E\left[r_i^c[n-\mu_1](r_i^c[n-\mu_2])^*\right] =& E\left[\sum_{t_1} h_i^c[t_1]r\left[(n-\mu_1)M-t_1-\beta\right]\cdot\sum_{t_2} h_i^c[t_2]r^*\left[(n-\mu_2)M-t_2-\beta\right]\right] \\
=& \sum_{t_1}\sum_{t_2} h_i^c[t_1]h_i^c[t_2]E\left[r\left[(n-\mu_1)M-t_1-\beta\right]\cdot r^*\left[(n-\mu_2)M-t_2-\beta\right]\right] \\
=& \sum_{t_1}\sum_{t_2} h_i^c[t_1]h_i^c[t_2]E\left[r\left[nM-\beta-(t_1+\mu_1 M)\right]\cdot r^*\left[nM-\beta-(t_2+\mu_2 M)\right]\right] \\
=& \sum_{t_1}\sum_{t_2} h_i^c[t_1]h_i^c[t_2]R_r\left(t_1+\mu_1 M, t_2+\mu_2 M\right),
\end{aligned}
\tag{A.2}
$$

and $R_r(t_1, t_2)$ is the noise autocorrelation between times t_1 and t_2. The other terms of (A.1) are

$$E\left[r_i^c[n-\mu_1](r_i^s[n-\mu_2])^*\right] = \sum_{t_1}\sum_{t_2} h_i^c[t_1]h_i^s[t_2]R_r\left(t_1+\mu_1 M, t_2+\mu_2 M\right), \tag{A.3}$$

and

$$E\left[r_i^s[n-\mu_1](r_i^s[n-\mu_2])^*\right] = \sum_{t_1}\sum_{t_2} h_i^s[t_1]h_i^s[t_2]R_r\left(t_1+\mu_1 M, t_2+\mu_2 M\right). \tag{A.4}$$

Therefore, the noise power yields

$$P_r(i) = \sum_{\mu_1=-L_A}^{L_A}\sum_{\mu_2=-L_A}^{L_A}\left[\sum_{t_1}\sum_{t_2} R_r\left(t_1+\mu_1 M, t_2+\mu_2 M\right)\right.$$
$$\left. \times \left(c_{i,\mu_1}c_{i,\mu_2}h_i^c[t_1]h_i^c[t_2] + s_{i,\mu_1}s_{i,\mu_2}h_i^s[t_1]h_i^s[t_2] + 2c_{i,\mu_1}s_{i,\mu_2}h_i^c[t_1]h_i^s[t_2]\right)\right]. \tag{A.5}$$

References

[1] T. Zheng, M. Raugi, M. Tucci, Time-invariant characteristics of naval power-line channels, IEEE Trans. Power Deliv. 27 (2) (2012) 858–865, https://doi.org/10.1109/TPWRD.2011.2181542.

[2] V. Degardin, P. Laly, M. Lienard, P. Degauque, Investigation on power line communication in aircrafts, IET Commun. 8 (10) (2014) 1868–1874.

[3] N. Taherinejad, L. Lampe, S. Mirabbasi, An adaptive impedance-matching system for vehicular power line communication, IEEE Trans. Veh. Technol. 66 (2) (2017) 927–940, https://doi.org/10.1109/TVT.2016.2562629.

[4] T. Gehrsitz, W. Kellerer, QoS and robustness of priority-based MAC protocols for the in-car power line communication, Veh. Commun. 9 (2017) 53–63.

[5] J. Yin, X. Zhu, Y. Huang, Y. Jiang, Null subcarriers assisted impulsive noise mitigation for in-vehicle power line communication in the presence of narrowband interference, IEEE Trans. Veh. Technol. 68 (1) (2019) 498–508, https://doi.org/10.1109/TVT.2018.2881145.

[6] M.T. Dabiri, S.M.S. Sadough, M.A. Khalighi, Blind signal detection under synchronization errors for FSO links with high mobility, IEEE Trans. Commun. 67 (10) (2019) 7006–7015.

[7] V. Degardin, I. Junqua, M. Lienard, P. Degauque, S. Bertuol, Theoretical approach to the feasibility of power-line communication in aircrafts, IEEE Trans. Veh. Technol. 62 (3) (2013) 1362–1366.

[8] IEEE Std 1901-2010, IEEE standard for broadband over power line networks: Medium access control and physical layer specifications, 2010, pp. 1–1586.

[9] F. Cruz-Roldán, F.A. Pinto–Benel, J.D.O. del Campo, M. Blanco–Velasco, A wavelet OFDM receiver for baseband power line communications, J. Franklin Inst. 353 (7) (2016) 1654–1671.

[10] H. Lin, P. Siohan, Capacity analysis for indoor PLC using different multi-carrier modulation schemes, IEEE Trans. Power Deliv. 25 (1) (2010) 113–124.

[11] P. Achaichia, M. Le Bot, P. Siohan, OFDM/OQAM: a solution to efficiently increase the capacity of future PLC networks, IEEE Trans. Power Deliv. 26 (4) (2011) 2443–2455, https://doi.org/10.1109/TPWRD.2011.2140341.

[12] L. Díez, J.A. Cortés, F.J. Cañete, E. Martos-Naya, S. Iranzo, A generalized spectral shaping method for OFDM signals, IEEE Trans. Commun. 67 (5) (2019) 3540–3551.

[13] F.A. Pinto-Benel, F. Cruz-Roldán, A bandpass wavelet OFDM system for power line communications, J. Franklin Inst. 357 (11) (2020) 7211–7228, https://doi.org/10.1016/j.jfranklin.2020.03.030.

[14] F.A. Pinto-Benel, M. Blanco-Velasco, F. Cruz-Roldán, Throughput analysis for wavelet OFDM in broadband power line communications, IEEE Access 6 (2018) 16727–16736.

[15] M. Zimmermann, K. Doster, Analysis and modeling of impulsive noise in broadband powerline communications, IEEE Trans. Electromagn. Compat. 44 (1) (Feb. 2002) 249–258.

[16] J.A. Cortés, L. Díez, F.J. Cañete, J. López, Analysis of the periodic impulsive noise asynchronous with the mains in indoor PLC channels, in: IEEE International Symposium on Power Line Communications and Its Applications, ISPLC, 2009.

[17] J.A. Cortés, L. Díez, F.J. Cañete, J.J. Sánchez-Martínez, Analysis of the indoor broadband power-line noise scenario, IEEE Trans. Electromagn. Compat. 52 (4) (2010) 849–858, https://doi.org/10.1109/TEMC.2010.2052463.

[18] A. Khan, S.Y. Shin, Linear precoded wavelet OFDM-based PLC system with overlap FDE for impulse noise mitigation, Int. J. Commun. Syst. 30 (17) (2017) e3349, https://doi.org/10.1002/dac.3349.

[19] N. Shlezinger, R. Shaked, R. Dabora, On the capacity of MIMO broadband power line communications channels, IEEE Trans. Commun. 66 (10) (2018) 4795–4810.

[20] Y.-R. Chien, H.-C. Yu, Mitigating impulsive noise for wavelet-OFDM powerline communication, Energies 12 (8) (2019), https://doi.org/10.3390/en12081567.

[21] A. Pittolo, M. De Piante, F. Versolatto, A.M. Tonello, In-vehicle power line communication: differences and similarities among the in-car and the in-ship scenarios, IEEE Veh. Technol. Mag. 11 (2) (2016) 43–51, https://doi.org/10.1109/MVT.2015.2480098.

[22] W.A. Martins, F. Cruz-Roldán, M. Moonen, P.S.R. Diniz, Intersymbol and intercarrier interference in OFDM transmissions through highly dispersive channels, in: 2019 27th European Signal Processing Conference (EUSIPCO), A Coruna, Spain, 2019, pp. 1–5.

[23] F. Cruz-Roldán, W.A. Martins, F. García-G, M. Moonen, P.S.R. Diniz, Intersymbol and intercarrier interference in OFDM systems: unified formulation and analysis, arXiv:2012.04527, 2020.

[24] F. García-Gangoso, M. Blanco-Velasco, F. Cruz-Roldán, Formulation and performance analysis of broadband and narrowband OFDM-based PLC systems, Sensors 21 (1) (2021), https://doi.org/10.3390/s21010290.

[25] F.A. Pinto-Benel, F. Cruz-Roldán, Exploring the performance of prototype filters for broadband PLC, in: 2017 IEEE International Symposium on Power Line Communications and Its Applications, ISPLC, 2017, pp. 1–6.

[26] H. Malvar, Signal Processing with Lapped Transforms, Artech House, Norwood MA, 1992.

[27] F.A. Pinto-Benel, F. Cruz-Roldán, 2-ASCET for broadband multicarrier transmission over in-home and in-vehicle power line networks, in: IEEE 18th International Conference on Intelligent Transportation Systems, 2015, pp. 1351–1356.

[28] M. Mohammadi, L. Lampe, M. Lok, S. Mirabbasi, M. Mirvakili, R. Rosales, P. van Veen, Measurement study and transmission for in-vehicle power line communication, in: Proc. IEEE ISPLC, Germany, 2009, pp. 73–78.

[29] J.A. Cortés, M. Cerdá, L. Díez, F.J. Cañete, Analysis of the periodic noise on in-vehicle broadband power line channels, in: IEEE International Symposium on Power Line Communications and Its Applications, 2012, pp. 334–339.